# LIM Kinase inhibitor Pyr1 reduces the growth and metastatic load of breast cancers

Chloé Prunier, Véronique Josserand, Julien Vollaire, Evelyne Beerling, Leanne De Koning, Christos Petropoulos, Olivier Destaing, Amandine Hurbin, Christopher Montemagno, Renaud Prudent, et al.

# LIM kinase inhibitor Pyr1 reduces the growth and metastatic load of breast cancers

*Chloé Prunier[1], Véronique Josserand[2], Julien Vollaire[2], Evelyne Beerling[3], Christos Petropoulos[4], Olivier Destaing[4], Christopher Montemagno[1], Amandine Hurbin[2], Renaud Prudent[1], Leanne de Koning[5],Reuben Kapur[6] Pascale A. Cohen[7], Corinne Albiges-Rizo[4], Jean-Luc Coll[2], Jacco van Rheenen[3], Marc Billaud[1] and Laurence Lafanechère[1]*

[1]*Univ. Grenoble Alpes, INSERM U823, Institut Albert Bonniot, Team "Polarity, Development and Cancer", Grenoble, France*

[2]*Univ. Grenoble Alpes, INSERM U823, Institut Albert Bonniot, Team " Cancer targets and experimental therapeutics", Grenoble, France*

[3]*Cancer Genomics Netherlands-Hubrecht Institute-KNAW and University Medical Center Utrecht; Utrecht, 3584 CT; the Netherlands.*

[4]*Univ. Grenoble Alpes, CNRS ERL5284, INSERM U823, Institut Albert Bonniot, Grenoble France*

[5]*Institut Curie, Translational Research Department, Paris, France*

[6]*Department of Pediatrics, Herman B Wells Center for Pediatric Research, Indiana University School of Medicine, Indianapolis, IN 46202, USA*

[7] *Univ. Lyon 1, INSERM U1052, CNRS UMR5286, Centre de Recherche en Cancérologie de Lyon, Lyon, France*

**Running title.** Pharmacological inhibition of LIM Kinases effect on breast tumors

**Keywords.** LIM Kinases, breast cancer, pyridocarbazolone, intravital imaging

Include the following notes on the title page (if applicable) in this order:

**Grant Support** This work was supported by the CNRS, the INSERM, and by grants from the Fondation de France and from Association Espoir for L.Lafanechère. It was supported by ANR Project Nanoluc ANR-11-BSV5-0018, France Life Imaging, French program "Investissement d'avenir"; Grant "Infrastructure d'avenir en biologie", ANR-11-INBS-0006 for J-L. Coll. and A. Hurbin. The RPPA platform is supported by the Cancéropôle Ile-de-France

C. Prunier was a PhD fellowship from the French Ministery of Research and from the French Foundation ARC. She was also the recipient of a subvention of Région Rhône-Alpes and of an EOLE grant.

R. Prudent was a post-doctoral fellowship from the French National Ligue against Cancer

C. Albiges-Rizo, C. Petropoulos. and O. Destaing were supported by LNCC.

**Disclosure of potential conflict of interest**

As shareholders of Cellipse S.A.S., L.Lafanechère and R. Prudent disclose a potential conflict of interest.

**Contact**

LAFANECHERE Laurence; PhD; Institut Albert Bonniot, CRI INSERM/UJF U823,

Team 3 "Polarity, Development and Cancer"

Site Santé

BP170

38042 Grenoble cedex 9 France

Phone: + (33) 476 54 95 71

e-mail: laurence.lafanechere@ujf-grenoble.fr

**Abstract**

LIM Kinases (LIMK) are emerging targets for cancer therapy and they function as network hubs to coordinate actin and microtubule dynamics. When LIMK are inhibited, actin microfilaments are disorganized and microtubules are stabilized. Owing to their stabilizing effect on microtubules, LIMK inhibitors may provide a therapeutic strategy to treat taxane-resistant cancers. In this study, we investigated the effect of LIMK inhibition on breast tumor development and on paclitaxel resistant tumors, using a novel selective LIMK inhibitor termed Pyr1. Treatment of breast cancer cells, including paclitaxel-resistant cells, blocked their invasion and proliferation *in vitro* and their growth *in vivo* in tumor xenograft assays. The tumor invasive properties of Pyr1 were investigated *in vivo* by intravital microscopy of tumor xenografts. A striking change of cell morphology was observed with a rounded phenotype arising in a subpopulation of cells, while other cells remained elongated. Notably, although Pyr1 decreased the motility of elongated cells it increased the motility of rounded cells in the tumor. Pyr1 administration prevented the growth of metastasis but not their spread. Overall, our results provided a preclinical proof of concept concerning how a small molecule inhibitor of LIMK kinases may offer a strategy to treat taxane-resistant breast tumors and metastases.

## Introduction

LIM Kinases (LIMK) regulate the architecture of the actin cytoskeleton by phosphorylation and inactivation of actin depolymerization factors of the ADF/cofilin family (1). Independently of this effect on actin microfilament dynamics, LIMK regulate microtubule dynamics (2–4), but whether this regulation occurs through a direct binding of LIMK to microtubules (5) or through phosphorylation of an associated protein (6) is still under debate. When LIMK are inhibited, microtubules are stabilized and actin microfilaments are severed and disorganized (2,4).

Thus, LIMK function as central network hubs coordinating several cellular- and tissue-level responses by regulating both actin microfilament and microtubule assembly (7). In pathophysiological conditions, pharmacological inhibition of LIMK could have antitumor and anti-metastatic effects, given the involvement of the actin and the microtubule cytoskeleton in cell division and in cell motility. The LIM kinase family of serine/threonine kinases includes two highly related members, LIMK1 and LIMK2 (1). LIMK activity is mainly regulated by the Rho-GTPases (RhoA, Rac and Cdc42) through their downstream kinases ROCK, PAK1, PAK4, and MRCK (1). The activation of the Rho-GTPases and their effectors, including LIMK, have been reported as playing important roles in tumor development and progression (8–13). Expression of LIMK or cofilin phosphorylation are elevated in malignant melanoma (14), glioma (15), prostate (4,16,17) and breast tumors (18,19). In breast cancer models, activation of LIMK is the last step of an integrin-linked machinery of cytoskeletal regulation that enables tumor initiation and metastatic colonization (20). Thus, LIMK are enzymes whose activity is elevated in cancers compared to normal tissue. Consequently, their inhibition could selectively target tumors and offer a large therapeutic window.

Chemotherapy is a component of the treatment of invasive breast cancers. One of the most important classes of chemotherapy agents is the taxanes, which bind and stabilize

microtubules. Taxane resistance, however, limits treatment options and creates a major challenge for clinicians. Taxane's general antimitotic and microtubule-stabilizing actions result also in severe side effects, such as myelosuppression or neurotoxicity. Rather than chemotherapeutic agents interacting directly with the microtubule network, the use of drugs that target microtubule regulators, such as LIMK, is hence an attractive alternative therapeutic strategy.

LIMK are considered as emerging targets for cancer therapy (21) and an increasing number of inhibitors is reported in the literature (2,22–28). Among these inhibitors, few, if any, fulfill the three criteria that are important for *in vivo* experiments, i.e. high selectivity, complete characterization of the effects on both actin and microtubule dynamics and knowledge of toxicity on animals.

We have previously identified and characterized a highly selective LIMK inhibitor, Pyr1 (2). Although ATP-competitive, Pyr1 inhibits only LIMK out of 110 kinases tested. When applied on cells, Pyr1 stabilizes microtubules, induces a cell cycle arrest at the S-G2/M phases and, through inhibition of cofilin phosphorylation, blocks actin microfilament dynamics. We have also shown that Pyr1 was active *in vitro* on paclitaxel sensitive and resistant cancerous cell lines and displayed a therapeutic activity in an *in vivo* murine model of leukemia L1210, while being well tolerated (2).

Because of the selectivity of this cell-permeable inhibitor and its good tolerance *in vivo*, the aims of this study were 1) to investigate the effect of LIMK inhibition on breast cancer development and 2) to test the hypothesis that LIMK inhibition is efficient in paclitaxel resistant cancers. The effects of Pyr1 on paclitaxel resistant breast cancers have been analyzed thoroughly, both *in vitro*, and *in vivo* on xenografted models of primary tumor growth and on metastasis. In response to Pyr1 treatment, intratumoral cell movement and tumor cell morphology have been monitored using intravital imaging. Our results show that Pyr1

displays an antitumoral activity. Intravital microscopy revealed morphological changes of the tumor cells and perturbation of their motile behavior within the tumor when treated with Pyr1. Finally, although Pyr1 did not prevent metastases, it led to an important reduction of the metastatic load. These results indicate that LIMK inhibitors might represent both a pharmacological alternative to the treatment of taxane resistant primary tumors and potent agents to reduce the growth of metastases.

## Material and Methods

### Cell culture

Murine mammary adenocarcinoma cells TS/A-pGL3 (20,29) and human cells MDA-MB-231 and MCF7 (American Type Culture Collection (ATCC), Manassas, VA, USA), routinely tested and authenticated by the ATCC, were cultured as recommended. MDA-MB-231 cells overexpressing the transcription factor ZNF217 (MDA-MB-231-ZNF217rvLuc2) were grown as previously described (30). For intravital microscopy experiments, MDA-MB-231 cells were modified in van Rheenen's team (for details, see supplementary information). MEF cells were a generous gift of Dr. Richard Hynes (Koch Institute for Integrative Cancer Research, MIT, USA). The expression of the constitutive active form of the Src kinase (SrcY527F) was performed as described in supplementary information.

**Western Blots** The antibodies used were from Cell Signaling Technology, i.e. Cofilin (ref. 5175), Phospho-Cofilin (ser3) (ref. 3313) and β-Actin (ref. 4967).

**Immunofluorescence analysis of the modification of cellular microtubule dynamics using nocodazole** was realized as previously described (2).

**Cell viability** was analyzed using MTT assay as previously described (2)**.**

**Matrigel invasion assay:** $5.10^4$ cells were plated on top of a layer of Matrigel in Transwell chambers (Biocoat, BD Biosciences). After 24 hours incubation with 25µM Pyr1 or 0.25%

DMSO, nuclei of cells that reached the bottom of the transwell were stained with Hoechst. Cell invasion was quantified by counting the number of invading cells using ImageJ software (NIH, Bethesda, MD, USA).

**FRAP analysis** was performed as described previously (31) on MEF SrcY527F cells transfected with GFP-Actin and treated or not with 25µM Pyr1 just before bleaching. Changes of fluorescent intensity within the bleached area were measured over 2 min and the characteristic time of recovery was quantified using the ZEN software from Zeiss.

**Wound Healing assay:** cells were seeded in culture inserts (ibidi, 80206). Two days later, inserts were removed and 25µM Pyr1 or 0.25% DMSO was added in the medium. Recovery of the wound was recorded during 12 hours using videomiscroscopy. Velocity, total displacement and persistence were calculated using the MTrackJ plugin (http://www.imagescience.org/meijering/software/mtrackj/manual/) from ImageJ software (NIH, Bethesda, MD, USA).

**Spheroids** were derived from MDA-MB-231 and MDA-MB-231-ZNF217rvLuc2 cells using the Matrigel-on-top culture as described in Shibue *et al.* (32). After five days of culture, spheroids were treated with 25µM Pyr1 or 0.25% DMSO. Filipodia number and length were quantified using an inverted microscope. A total of 25 -from 3 different experiments was analyzed in each group.

***In vivo* experiments:** all animal studies were conducted in accordance with European Union guidelines and approved by the regional ethics committee. The animals were examined daily for mortality and morbidity. Weight was monitored twice a week and behavior was carefully examined every day from the beginning of treatments (grooming, postures, spontaneous movement in the cage and touch response)

Populations of $5x10^5$ TS/A-pGL3 cells, stably transfected with luciferase, were suspended in PBS and injected into the mammary fat pad of thirty NMRI nude mice. Seven days later, mice were randomized in 3 equal groups and drugs (Pyr1- synthesized by C-H Nguyen, Institut Curie, France- 10 mg/Kg, PTX (Sigma, T1912, 10 mg/Kg) or vehicle (36% PEG 400, 10% DMSO and 54% NaCl 0.9%) were daily-injected intraperitoneally. Tumor growth was monitored by bioluminescence twice a week. Before each bioluminescence imaging (IVIS Kinetic; Caliper), anesthetized mice received an intraperitoneal injection of Luciferin (Promega).

Populations of $10x10^6$ MDA-MB-231 cells were suspended in PBS/Matrigel v/v (BD Biosciences) and injected subcutaneously, into the right flank of thirty NMRI nude mice. When tumors were palpable i.e. twenty-one days after cell injection, mice were randomized in 3 equal groups and drugs were daily-injected intraperitoneally, as described above. Tumor growth was monitored three times a week with a sliding caliper.

Populations of $5x10^5$ MDA-MB-231 Dendra2 cells were suspended in PBS and injected into the mammary fat pad of 7 females NSG. A first group (4 mice) was injected with 10 mg/Kg Pyr1 and a second (3 mice) with vehicle (36% PEG 400, 10% DMSO and 54% NaCl 0.9%). Treatments were daily-injected intraperitoneally and started between thirty and forty-five days after cell injection, i.e. when tumors were palpable and window implanted. Imaging sessions started two days after mammary window implantation. Each session lasted 2 hours with one stack every 15 minutes. Each mouse was imaged twice a week during two weeks. Mice were anesthetized and intravital imaging was achieved as described previously (33). Details of the methods used for tumoral cells migration tracking and for quantification of fluorescent signal in MDA MB 231 Dendra2 tumors are presented in supplementary information.

Populations of $2.5x10^5$ MDA-MB-231-ZNF217rvLuc2 cells stably transfected with luciferase were suspended in PBS and injected in the left ventricle of 40 NMRI nude mice. The quality of cell implantation was checked immediately after injection by bioluminescence and only mice with validated implantation were included in the experiment. Treatments started 3 days before cell injection. A first group of 15 mice was daily-injected intraperitoneally with 10 mg/Kg Pyr1 and a second of 9 mice was injected with vehicle (36% PEG 400, 10% DMSO and 54% NaCl 0.9%). Metastatic colonization was monitored by bioluminescence, as described above.

**Ki67 staining:** MDA-MB-231 Dendra2 tumors were fixed O/N at 4°C in periodate-lysine paraformaldehyde (PLP) buffer (4% PFA 2.5 ml, $NaIO_4$ 0.0212 g, L-Lysine 3.75 ml, P-buffer pH 7.4 3.75 ml). The fixed tissues were then washed twice with PLP buffer and placed for 6 hours in 30% sucrose at 4°C. Tumors were embedded in OCT tissue freezing medium (Jung). Tumor sections (14µm) were incubated with Ki67 antibody (Abcam, 66155) overnight and then with A647-conjugated secondary antibody. Proliferation was evaluated as the number of Ki67 positive cells per field ± SEM. A total of six fields was examined and counted for each tumor in each group.

**TUNEL** labeling was performed using *in situ* cell death detection kit (Invitrogen, C10247). Tumor sections (14µm) were counterstained with Hoechst. The apoptotic index corresponded to the number of TUNEL positive cells per field. A total of six fields was examined and counted for each tumor in each group.

**Statistical analyses:** statistical analyses were performed using t-test except for tumor growth and cell migration *in vivo* experiments for which a Mann-Whitney test was used. Results with probability values < 0.05 were considered to be statistically significant.

## Results

### Pyr1 treatment decreases cancer breast cell proliferation *in vitro*

As the expression level of LIMK1 and its activity have been reported to be increased in invasive breast cancer cells (34,35), we first characterized the different cell lines used in this study, i.e. TS/A-pGL3, MDA-MB-231 and MDA-MB-231-ZNF217rvLuc2, regarding their level of expression of LIMK1. Using Western blotting, we found that the endogenous level of LIMK1 was at least 50% higher in these invasive cell lines, as compared to MCF-7 cells, a non-invasive cell line ((34,36), **Supplementary Fig. 1A,B**).

These cell lines have been described to show resistance to PTX (37–39). We confirmed that PTX had almost no effect on TS/A-pGL3 cell viability and reduced MDA-MB-231 and MDA-MB-231-ZNF217rvLuc2 cell viability by only 30-40% over 24-48h, relative to vehicle control (**Supplementary Fig.2**).

We then tested if the LIMK inhibitor Pyr1 was active on these cell lines by measuring its effect on cofilin phosphorylation and on microtubule dynamics. Cofilin phosphorylation was quantified by Western blotting and slowing down of microtubule dynamics was assessed by evaluation of the resistance of the microtubule network to nocodazole-induced depolymerization. Nocodazole binds free tubulin and prevents its incorporation into microtubules, inducing microtubule depolymerization. Stabilized microtubules, with slow dynamics, have reduced exchanges with the free tubulin pool and are thus less sensitive to nocodazole-induced depolymerization (2).

Although showing some variation between cell lines, Pyr1 consistently inhibited cofilin phosphorylation, in a dose dependent manner (**Fig. 1A**). Moreover, Pyr1 protected the microtubule network from nocodazole-induced depolymerization (**Fig. 1B**), indicating that microtubules were stabilized.

We then analyzed the toxicity of Pyr1 on these cell lines. Toxicity profiles were obtained by determining population cell viability in response to a 48-hour incubation with Pyr1 (0 to 25 µM). As shown in **Figure 1C**, Pyr1 has a significant effect on the proliferation of these cell lines, reducing their viability by about 90 %. The $GI_{50}$ (50% of growth inhibition) of Pyr1 was 1.4 µM for TS/A-pGL3, 3.9 µM for MDA-MB-231 and 7 µM for MDA-MB-231-ZNF217rvLuc2.

Thus, *in vitro*, Pyr1 affects the proliferation of invasive cells that exhibit resistance to PTX.

**Pyr1 treatment of xenograft tumor bearing mice induces a significant decrease of tumor size**

Since Pyr1 affects the *in vitro* proliferation of mammary and breast cancer cell lines, we further analyzed its effect on tumors xenografted to mice and compared it to the PTX effect, administrated at a therapeutic dose (40).

While Pyr1 did not induce detectable adverse effects (**Supplementary Figure 3**), PTX-treated mice were motionless, displayed swollen abdomen and lost weight after two weeks of treatment. This led to the arrest of the experiment for ethical issues. Consistent with the *in vitro* cell viability results, PTX was unable to stop the growth of TS/A-pGL3 tumors whereas Pyr1 stopped their growth (**Fig. 2A, B**).

Pyr1 contains an ester moiety, which could be subjected to hydrolysis *in vivo*. We thus analyzed the intravenous concentration of Pyr1 and of its 9-OH metabolite M1, lacking the ester moiety, after a single i.p. injection of 10 mg/Kg of Pyr1. We found that 25 min after the

initial injection Pyr1 was undetectable in the blood whereas its metabolite M1 was present. M1 concentration decreased progressively to reach its basal level within 2 hours (**Supplementary Fig. 4**). This is in line with the high distribution volume, which indicates that compounds exit quickly from the plasmatic compartment. As we have shown that M1 is also able to inhibit LIMK, both *in vitro* and in cells (Compound 3, (2)), we hypothesize that the observed effect results mainly from the combined action of Pyr1 and its 9-OH metabolite. For the sake of clarity, the generic term Pyr1 will be further used to refer to Pyr1 and its metabolite.

Tumors were excised at the end of the experiment and several markers related to microtubule and actin regulation (**Supplementary Table 1**) were quantified using a Reverse Phase Protein Array (RPPA). Among these markers, the level of phospho-cofilin in tumors was not significantly different between Pyr1-treated mice and vehicle-treated mice. The levels of acetylated- and detyrosinated-tubulin, which are indirect markers of microtubule stabilization (2), were found significantly increased in Pyr1-treated mice, as compared with the vehicle-treated mice. Such an increase was not detected in the tumors of PTX-treated mice, which could be correlated with the absence of a PTX effect on tumor growth (**Supplementary Figure 5**). These results strongly suggest that the Pyr1 effect in tumors involves microtubule stabilization.

Next, the effect of Pyr1 and PTX on subcutaneous MDA-MB-231 xenografts was also compared. When the tumors reached a palpable size (200-300 $mm^3$), Pyr1 and PTX were daily injected. As for TS/A-pGL3 experiments, the end-point of the experiment was governed by PTX-induced side effects. Pyr1, as well as PTX, induced a statistically significant decrease (40%-50%) of the tumor volume (**Fig. 2C**).

Tumors were excised at the end of the experiment and cut in two pieces. One piece was used to analyze the structure of the tumors. Hematoxylin and eosin staining of the tumor sections

showed that the cellular density of Pyr1- and PTX- treated tumors was greatly reduced, confirming the antitumor effect of these compounds (**Supplementary Figure 6)**.

The phosphorylated-cofilin and the detyrosinated-tubulin contents were analyzed by Western blotting, using the other piece, and quantified. Whereas no statistical difference was observed when comparing the level of phosphorylated-cofilin in vehicle- and Pyr1- or PTX-treated tumors, a consistent enhancement of the level of detyrosinated-tubulin was observed in Pyr1- and PTX- treated tumors (**Supplementary Figure 7**). Again, this suggests that the antitumor effect of the PTX and Pyr1 involved a stabilization of microtubules.

Taken together, these results indicate that Pyr1 has a potent anti-tumor effect on primary mammary tumors in breast cancer models, even on PTX resistant tumors such as TS/A-pGL3.

**Pyr1 treatment inhibits the invasive migration of breast cancer cell lines and the formation of filopodium-like protrusions *in vitro***

It has been shown that interfering with LIMK function either by using RNAi (16) or by overexpression of a dominant negative form of LIMK1 in metastatic breast cancer cells (34), or by pharmacological LIMK inhibition (41) results in reduced cell invasiveness.

Moreover, as LIMK expression is correlated with the aggressiveness of cancer cells (13,19,20) we decided to investigate if LIMK inhibition by Pyr1 impacted TS/A-pGL3, MDA-MB-231 and MDA-MB-231-ZNF217rvLuc2 invasiveness *in vitro*.

We examined the Pyr1 effect on the motility of cells using a wound-healing assay. We observed that Pyr1 significantly reduced the motility of the three cell lines (**Fig. 3A**). After tracking the cells individually, we found that Pyr1 reduced the speed of cell movement by ~ 75%. The total displacement was reduced at least by 50%. Pyr1 also reduced the directionality of the cell movement (**Fig. 3B**).

We then analyzed the Pyr1 effect on invasive migration of these cells through matrigel in Transwell chambers. Cells were seeded in the insert of the chambers and after 24 hours, the nuclei of invasive cells were counted. As shown in **Figure 3C**, Pyr1 exerted a strong inhibitory effect on the invasion of the three cell lines.

Invasion involves specialized finger-like actin structures, called invadosomes in cancer cells, that can be induced by the expression of a constitutively active form of Src (42). These structures self-assemble into round metastructures known as rosettes or rings (31). We investigated the effect of LIMK inhibition on actin dynamics in invadosomes using MEF cells expressing a constitutively active form of Src (Src Y527F) and life-act RFP.

We first observed that cells treated for 2h with 25 μM of Pyr1 showed disorganized invadosomes. Instead of the normal ring structure, the actin cytoskeleton was often reorganized into actin spots, indicating that actin dynamics was perturbed (**Fig. 3D**). FRAP analysis of the few remaining invadosomes after Pyr1 treatment allowed measuring the net flux of GFP-actin into these structures. We found that the time of recovery doubled in invadosomes of Pyr1 treated cells compared to control cells, indicating that actin dynamics was strongly slowed down (**Fig. 3E, Supplementary Movie 1**). This result suggests that the cyclic phosphorylation/dephosphorylation of cofilin is central for actin dynamics in invadosomes (43) and that complete blockade of cofilin phosphorylation through LIMK inhibition leads to unbalanced actin dynamics.

We conclude from these experiments that, *in vitro*, Pyr1 is able to slow down cell motility and to suppress invasion.

We further explored the consequences of LIMK inhibition in the processes that allow the survival and proliferation of cancer cells after their settling in the parenchyma of distant tissues. It has been shown that the ability of breast cancer cell lines to settle in a foreign tissue is determined by their capacity to extend abundant actin-rich protrusions morphologically

resembling filipodia, called filipodium-like protrusions (FLPs), when cultured in three dimensions (36). The activation of the ILK/β-parvin/cofilin pathway leads to the activation of LIMK to govern FLPs lifetime (20). Blocking this pathway, through the production of constitutively active cofilin has been shown to impair FLPs formation (20). We wondered whether pharmacological inhibition of LIMK could also impact on FLPs formation. MDA-MB-231 and MDA-MB-231-ZNF217rvLuc2 cells were thus propagated in 3-dimensional cultures using the "Matrigel-on-top" method (36), in which cells are plated above a layer of 100% matrigel and then covered with culture medium containing 2% matrigel. In such conditions, these cells grow as spheroids. We found that about half of MDA-MB-231 and MDA-MB-231-ZNF217rvLuc2 spheroids extend FLPs. After a two-hour treatment with 25μM of Pyr1, the percentage of spheroids with FLPs was reduced to 39 % for MDA-MB-231 and to 33% for MDA-MB-231-ZNF217rvLuc2 cells (**Fig. 4 A, B**). We measured the length of the remaining FLPs and found that they were reduced by 37% for both MDA-MB-231 and MDA-MB-231-ZNF217rvLuc2 cells (**Fig. 4C**). Thus, pharmacological inhibition of LIMK has a profound effect on FLPs abundance and length.

**Pyr1 increases tumor cell velocity *in vivo***

As the velocity properties of cell motility *in vivo* are often different from that observed on two dimensional substrates (44,45), we then investigated the Pyr1 effect on tumor cell motility *in vivo*, using intravital imaging. MDA-MB-231 cells expressing the Dendra2 fluorescent protein were implanted into murine mammary fat pads. When the tumors were palpable, i.e. 30 to 45 days after implantation, mammary imaging windows were surgically implanted. Mice were then daily injected with 10 mg/Kg of Pyr1. As shown in **Figure 5A** and in **Supplementary Movies 2 and 3**, acquired images indicated that cells in the tumors of mice treated with Pyr1 for at least 8 days were less packed than cells in the tumors of the vehicle-

treated mice. To quantify this effect, we measured the area covered by fluorescent cells. We found that there were statistically less fluorescent cells in tumors of mice treated with Pyr1 (**Fig. 5B**). These results are consistent with the reduced number of tumor cells observed in the above-described experiment on subcutaneous MDA-MB-231 xenografts treated with Pyr1 (**Supplementary Fig. 6).** Indeed, cell proliferation, as assessed by Ki67 staining and quantification, was significantly decreased in tumors of Pyr1 treated mice (**Fig. 5C)**, whereas the number of apoptotic cells, detected with TUNEL staining, was significantly increased in these tumors **(Fig. 5D**). These observations confirmed the anti-tumor effect of Pyr1.

Even though the measurement of cell velocity within the tumor did not show any significant difference upon Pyr1 treatment (**Fig. 6A**), cell morphology was affected. Whereas 90% of cells in vehicle treated mice are elongated, 60% of cells displayed a rounded morphology in Pyr1 treated mice (**Fig. 5A, Fig. 6B**). The migratory properties of elongated and rounded cells were separately analyzed. Pyr1 treatment induced a significant decrease of both the velocity and the distance covered by elongated cells, as compared to vehicle treated cells (**Fig. 6C, D**). In contrast the velocity of rounded cells almost doubled. The total distance covered by rounded cells was three times higher and their persistence was lower upon Pyr1 treatment, as compared to elongated cells (**Fig. 6 C, D, E, F**).

Altogether, our results indicate that *in vivo* Pyr1 treatment increases the velocity of cell movements in the tumor.

**Pyr1 impairs the growth of metastases.**

If Pyr1 treatment increases the velocity of malignant cells, it is expected that the migration of the cells and the establishment of distant metastases will be enhanced. Dendra2 protein expression in cells allowed the *postmortem* evaluation of the colonization of distant organs by tumor cells at the end of the intravital imaging experiment. Quantification of the fluorescent

cells in lung cryosections indicated that Pyr1 treatment did not affect the number of metastases, contrary to expectation (**Fig. 7A, B**). The size of the metastases was however significantly reduced by Pyr1 treatment since the number of cells per metastasis in Pyr1 treated mice was decreased by 90% (**Fig. 7A, C**), confirming the strong effect of Pyr1 on cell proliferation.

To further explore the impact of Pyr1 on *in vivo* metastatic colonization, the aggressive MDA-MB-231-ZNF217rvLuc2 cells (30) were injected directly into the blood stream of Pyr1 treated mice and control mice. Bioluminescence imaging demonstrated that although Pyr1 did not affect the number of metastases, it has a clear impact on the global metastatic load (**Fig. 7D, E, F**). Interestingly, this effect was long lasting, as the global metastatic load did not rise steeply even 12 days after the end of the treatment (**Fig. 7E**). We conclude from this experiment that Pyr1 treatment had no effect on metastasis establishment but induced a strong reduction of metastases growth.

**Discussion**

In the Rho pathway, LIMK are the most distal kinases that directly control microtubule and actin dynamics. This position in the signaling network makes them attractive targets for pharmacological inhibition in a therapeutic perspective. In this study, we have explored the efficacy of the LIMK inhibitor Pyr1 on breast cancers and compared the effects of Pyr1 with those of PTX. We found that Pyr1 was effective on PTX resistant tumors, leading to the reduction of tumor size, with no detectable adverse side effects on mice. Assessing the mechanism of action of a new therapeutic agent is important (46). In contrast to our *in vitro* results we could not detect a statistically significant decrease of the level of cofilin phosphorylation in Pyr1-treated tumors. Several explanations may account for these differences. First, cofilin phosphorylation was measured on whole tumor extracts and putative

intratumor differences may have been overlooked. Alternatively, since the behavior of cells, including the migration properties, *in vivo* are often different from that observed on two dimensional substrates (44,45), it is possible that the differences in cofilin phosphorylation and cell migration velocities are due to the 2D *in vitro* and the 3D *in vivo* assay systems. In contrast, we found that the amount of detyrosinated tubulin was systematically enhanced in Pyr1 treated tumors, but such an enhancement that occurs upon a null background of detyrosinated tubulin may be easier to detect than a decrease of a normally expressed marker such as phospho-cofilin.

Although we do not exclude the possibility that Pyr1 exerts its antitumor effect through a modification of actin microfilament dynamics, our data show that its effect strongly correlates with the stabilization of the microtubule network.

The assembly and disassembly of actin in cellular structures, such as lamellipodia and filopodia is not only regulated by LIMK but has been postulated to be an integral component of LIMK-regulated cell invasion (20,21). We have analyzed Pyr1 effects, both *in vitro* and *in vivo,* on cell motility and invasion. We found that although Pyr1 inhibits *in vitro* cell motility, its effect is more complex *in vivo*. Firstly, tumors treated with Pyr1 were heterogeneous, comprising two tumor cell populations,: cells with a rounded morphology and cells with an elongated morphology. Secondly, motility differed according to the cell shape: upon Pyr1 treatment, the motility of elongated cells decreased while the motility of rounded cells increased. This heterogeneity likely reflects the variations of intratumoral Pyr1 concentrations which generate two different phenotypic outcomes that differ by their cell motility and cell shape features (47,48).

The disparity between *in vitro* and *in vivo* observations, regarding the effect of Pyr1 on cell motility could have other explanations. Besides differences in drug dosing, differences in the duration of *in vivo* treatment and of *in vitro* assay could be at the origin of this disparity.

The change of cell shape and motility parameters observed in Pyr1-treated tumors could also result from modifications of the biomechanical properties of interstitial tissue(49). More generally, a global effect of Pyr1 on the tumor microenvironment could perturb the fine balance between chemical and mechanical signals produced by the different cell types and thus modify the shape and the motility phenotype of tumor cells (50).

Overall, although *in vitro* Pyr1 has both an anti-proliferative and anti migration effect, *in vivo* experiments indicate that the anti-proliferative effects of the drug are stronger than the migration effects.

Although Pyr1 did not inhibit *in vivo* tumor cell migration and metastasis seeding, we consistently observed that the size of the metastases remained small, regardless whether the cells migrated from the primary tumor or whether they were directly injected into the circulation. Our observations indicate that pharmacological inhibition of LIMK impairs the proliferation of cancer cells at their new sites of implantation. These findings are consistent with the results obtained by Shibue *et al.*, following experimental implantation of breast cancer cells bearing a constitutively active cofilin mutant that mimics an inhibition of LIMK (20).

Taken together our data indicate that LIMK inhibitors, such as Pyr1, could represent potent agents to decrease the growth of both primary tumors and their metastasis. Moreover, they are a possible pharmacological alternative to overcome the tumor resistances frequently observed when patients are treated with taxanes.

**Acknowledgments**

The authors thank C.H. Nguyen for Pyr1 synthesis, C. Lecerf, F. Bard and A. Barbet for performing the RPPA experiments, M. Barreto from SimplicityBio for statistical analysis, P. Poullet et S. Liva for RPPA data representation, A. Zomer and M. Alieva for technical help for intravital microscopy, K. Sadoul for critical reading of the manuscript.

**References**

1. Scott RW, Olson MF. LIM kinases: function, regulation and association with human disease. J Mol Med. 2007;85:555–68.
2. Prudent R, Vassal-Stermann E, Nguyen CH, Pillet C, Martinez A, Prunier C, et al. Pharmacological inhibition of LIM kinase stabilizes microtubules and inhibits neoplastic growth. Cancer Res. 2012;72:4429–39.
3. Gorovoy M, Niu J, Bernard O, Profirovic J, Minshall R, Neamu R, et al. LIM kinase 1 coordinates microtubule stability and actin polymerization in human endothelial cells. J Biol Chem. 2005;280:26533–42.
4. Elevated LIM Kinase 1 in Nonmetastatic Prostate Cancer Reflects Its Role in Facilitating Androgen Receptor Nuclear Translocation. Mol Cancer Ther. 2015; 14:246-58.
5. Bhardwaj A, Srivastava SK, Singh S, Arora S, Tyagi N, Andrews J, et al. CXCL12/CXCR4 signaling counteracts docetaxel-induced microtubule stabilization via p21-activated kinase 4-dependent activation of LIM domain kinase 1. Oncotarget. 2014; 5:11490-500.
6. Pleines I, Dütting S, Cherpokova D, Eckly A, Meyer I, Morowski M, et al. Defective tubulin organization and proplatelet formation in murine megakaryocytes lacking Rac1 and Cdc42. Blood 2013;122:3178–87.
7. Fife CM, McCarroll JA, Kavallaris M. Movers and shakers: cell cytoskeleton in cancer metastasis. Br J Pharmacol. 2014;171:5507–23.
8. Molecular Pathways: Targeting the Kinase Effectors of RHO-Family GTPases.
9. Mali RS, Kapur R. Targeting Rho associated kinases in leukemia and myeloproliferative neoplasms. Oncotarget. 2012;3:909–10.
10. Sahai E, Marshall CJ. RHO-GTPases and cancer. Nat Rev Cancer. 2002;2:133–42.
11. Rath N, Olson MF. Rho-associated kinases in tumorigenesis: re-considering ROCK inhibition for cancer therapy. EMBO Rep. 2012;13:900–8.
12. Manetti F. LIM kinases are attractive targets with many macromolecular partners and only a few small molecule regulators. Med Res Rev. 2012;32:968–98.

13. Wang W, Goswami S, Lapidus K, Wells AL, Wyckoff JB, Sahai E, et al. Identification and testing of a gene expression signature of invasive carcinoma cells within primary mammary tumors. Cancer Res. 2004;64:8585–94.

14. Okamoto I, Pirker C, Bilban M, Berger W, Losert D, Marosi C, et al. Seven novel and stable translocations associated with oncogenic gene expression in malignant melanoma. Neoplasia. 2005;7:303–11.

15. Park J-B, Agnihotri S, Golbourn B, Bertrand KC, Luck A, Sabha N, et al. Transcriptional profiling of GBM invasion genes identifies effective inhibitors of the LIM kinase-Cofilin pathway. Oncotarget. 2014;5:9382–95.

16. Davila M, Frost AR, Grizzle WE, Chakrabarti R. LIM kinase 1 is essential for the invasive growth of prostate epithelial cells: implications in prostate cancer. J Biol Chem. 2003;278:36868–75.

17. Ahmed T, Shea K, Masters JRW, Jones GE, Wells CM. A PAK4-LIMK1 pathway drives prostate cancer cell migration downstream of HGF. Cell Signal. 2008;20:1320–8.

18. McConnell B V, Koto K, Gutierrez-Hartmann A. Nuclear and cytoplasmic LIMK1 enhances human breast cancer progression. Mol Cancer. 2011;10:75.

19. Bagheri-Yarmand R, Mazumdar A, Sahin AA, Kumar R. LIM kinase 1 increases tumor metastasis of human breast cancer cells via regulation of the urokinase-type plasminogen activator system. Int J Cancer. 2006;118:2703–10.

20. Shibue T, Brooks MW, Weinberg RA. An integrin-linked machinery of cytoskeletal regulation that enables experimental tumor initiation and metastatic colonization. Cancer Cell. 2013;24:481–98.

21. Manetti F. Recent Findings Confirm LIM Domain Kinases as Emerging Target Candidates for Cancer Therapy. Curr. Cancer Drug Targets. 2012. page 543–60.

22. Ross-Macdonald P, de Silva H, Guo Q, Xiao H, Hung CY, Penhallow B, et al. Identification of a nonkinase target mediating cytotoxicity of novel kinase inhibitors. Mol Cancer Ther. 2008;7:3490–8.

23. Harrison BA, Whitlock NA, Voronkov M V, Almstead ZY, Gu KJ, Mabon R, et al. Novel class of LIM-kinase 2 inhibitors for the treatment of ocular hypertension and associated glaucoma. J Med Chem. 2009;52:6515–8.

24. Harrison BA, Almstead ZY, Burgoon H, Gardyan M, Goodwin NC, Healy J, et al. Discovery and Development of LX7101, a Dual LIM-Kinase and ROCK Inhibitor for the Treatment of Glaucoma. ACS Med Chem Lett. 2015;6:84–8.

25. Ohashi K, Sampei K, Nakagawa M, Uchiumi N, Amanuma T, Aiba S, et al. Damnacanthal, an effective inhibitor of LIM-kinase, inhibits cell migration and invasion. Mol Biol Cell. 2014;25:828–40.

26. Mashiach-Farkash E, Rak R, Elad-Sfadia G, Haklai R, Carmeli S, Kloog Y, et al. Computer-based identification of a novel LIMK1/2 inhibitor that synergizes with salirasib to destabilize the actin cytoskeleton. Oncotarget. Impact Journals, LLC; 2012;3:629–39.

27. Rak R, Haklai R, Elad-Tzfadia G, Wolfson HJ, Carmeli S, Kloog Y. Novel LIMK2 Inhibitor Blocks Panc-1 Tumor Growth in a mouse xenograft model. Oncoscience.

Impact Journals, LLC; 20141:39–48.

28. Yin Y, Zheng K, Eid N, Howard S, Jeong J-H, Yi F, et al. Bis-aryl Urea Derivatives as Potent and Selective LIM Kinase (Limk) Inhibitors. J Med Chem. American Chemical Society; 2015; 58:1846-61.

29. Nanni P, de Giovanni C, Lollini PL, Nicoletti G, Prodi G. TS/A: a new metastasizing cell line from a BALB/c spontaneous mammary adenocarcinoma. Clin Exp Metastasis. 1:373–80.

30. Vendrell JA, Thollet A, Nguyen NT, Ghayad SE, Vinot S, Bièche I, et al. ZNF217 is a marker of poor prognosis in breast cancer that drives epithelial-mesenchymal transition and invasion. Cancer Res. 2012;72:3593–606.

31. Albiges-Rizo C, Destaing O, Fourcade B, Planus E, Block MR. Actin machinery and mechanosensitivity in invadopodia, podosomes and focal adhesions. J Cell Sci. 2009;122:3037–49.

32. Shibue T, Weinberg RA. Integrin beta1-focal adhesion kinase signaling directs the proliferation of metastatic cancer cells disseminated in the lungs. Proc Natl Acad Sci U S A. 2009;106:10290–5.

33. Zomer A, Ellenbroek SIJ, Ritsma L, Beerling E, Vrisekoop N, Van Rheenen J. Intravital imaging of cancer stem cell plasticity in mammary tumors. Stem Cells. 2013;31:602–6.

34. Yoshioka K, Foletta V, Bernard O, Itoh K. A role for LIM kinase in cancer invasion. Proc Natl Acad Sci U S A. 2003;100:7247–52.

35. Wang W, Eddy R, Condeelis J. The cofilin pathway in breast cancer invasion and metastasis. Nat Rev Cancer. 2007;7:429–40.

36. Shibue T, Brooks MW, Inan MF, Reinhardt F, Weinberg RA. The outgrowth of micrometastases is enabled by the formation of filopodium-like protrusions. Cancer Discov. 2012;2:706–21.

37. Thollet A, Vendrell JA, Payen L, Ghayad SE, Ben Larbi S, Grisard E, et al. ZNF217 confers resistance to the pro-apoptotic signals of paclitaxel and aberrant expression of Aurora-A in breast cancer cells. Mol Cancer. 2010;9:291.

38. Flores ML, Castilla C, Ávila R, Ruiz-Borrego M, Sáez C, Japón MA. Paclitaxel sensitivity of breast cancer cells requires efficient mitotic arrest and disruption of Bcl-xL/Bak interaction. Breast Cancer Res Treat. 2012;133:917–28.

39. Janát-Amsbury MM, Yockman JW, Lee M, Kern S, Furgeson DY, Bikram M, et al. Combination of local, nonviral IL12 gene therapy and systemic paclitaxel treatment in a metastatic breast cancer model. Mol Ther. 2004;9:829–36.

40. Riondel J, Jacrot M, Picot F, Beriel H, Mouriquand C, Potier P. Therapeutic response to taxol of six human tumors xenografted into nude mice. Cancer Chemother Pharmacol. 1986;17:137–42.

41. Mardilovich K, Baugh M, Crighton D, Kowalczyk D, Gabrielsen M, Munro J, et al. LIM kinase inhibitors disrupt mitotic microtubule organization and impair tumor cell proliferation. Oncotarget. 2015; 6:38469-86.

42. Destaing O, Planus E, Bouvard D, Oddou C, Badowski C, Bossy V, et al. β1A integrin is a master regulator of invadosome organization and function. Mol Biol Cell.

2010;21:4108–19.

43. Bravo-Cordero JJ, Magalhaes MAO, Eddy RJ, Hodgson L, Condeelis J. Functions of cofilin in cell locomotion and invasion. Nat Rev Mol Cell Biol. NIH Public Access; 2013;14:405–15.

44. Entenberg D, Kedrin D, Wyckoff J, Sahai E, Condeelis J, Segall JE. Imaging tumor cell movement in vivo. Curr Protoc Cell Biol 2013;Chapter 19:Unit19.7.

45. Beerling E, Ritsma L, Vrisekoop N, Derksen PWB, van Rheenen J. Intravital microscopy: new insights into metastasis of tumors. J Cell Sci. 2011;124:299–310.

46. Bunnage ME, Chekler ELP, Jones LH. Target validation using chemical probes. Nat Chem Biol. 2013;9:195–9.

47. Wang W, Mouneimne G, Sidani M, Wyckoff J, Chen X, Makris A, et al. The activity status of cofilin is directly related to invasion, intravasation, and metastasis of mammary tumors. J Cell Biol. 2006;173:395–404.

48. Etienne-Manneville S. Microtubules in cell migration. Annu Rev Cell Dev Biol. 2013;29:471–99.

49. Wolf K, Friedl P. Extracellular matrix determinants of proteolytic and non-proteolytic cell migration. Trends Cell Biol. 2011;21:736–44.

50. Gligorijevic B, Bergman A, Condeelis J. Multiparametric classification links tumor microenvironments with tumor cell phenotype. PLoS Biol. 2014;12:e1001995.

**Legends for figures**

**Figure 1**: ***In vitro*** **characterization of Pyr1 effects on invasive PTX resistant breast cancer cell lines**.

**A**. Pyr1 effects on cofilin phosphorylation. Cells were treated for 2 hours with 0.25% DMSO, 10µM or 25µM Pyr1, as indicated. Lysates (15 µg of proteins) were blotted for phospho-Cofilin (P-Cofilin) or Cofilin.

**B**. Pyr1 effect on microtubule resistance to nocodazole-induced depolymerization. Cells were incubated with 25µM Pyr1 or 0.25% DMSO before nocodazole (10µM) addition. They were then stained for tubulin. Bar, 10µm.

**C.** Pyr1 effect on the viability of breast cancer cell lines. Cells were incubated for 48 hours with Pyr1. The percentage of viable cells was calculated following MTT assay.

**Figure 2**: **Pyr1 effects on tumor development of murine (TS/A-pGL3) allografts and human (MDA-MB-231) xenografts**.

**A**. Pyr1 inhibits the growth of orthotopic TS/A-pGL3 allografts. TS/A-pGL3 cells that stably express luciferase were injected into the mammary gland. Seven days after inoculation, mice were randomized and daily treated with Pyr1 (10 mg/Kg, i.p.), PTX (10 mg/Kg, i.p.) or vehicle for 14 days. Bioluminescence imaging was performed twice a week. Bars = SEM, n = 10 mice per group, * $p < 0.05$.

**B**. Overtime bioluminescence images of TS/A-pGL3 allografts (one representative mouse per condition).

**C**. Pyr1 reduces the size of subcutaneous MDA-MB-231 xenografts. MDA-MB-231 cells were injected into the flank. Twenty-one days after inoculation, mice were treated with Pyr1 (10 mg/Kg, i.p.), PTX (10 mg/Kg, i.p.) or vehicle. Tumor size was measured twice a week. Values are expressed as percentage of the measured value at day 21. Bars = SEM, n = 10 mice per group, * $p < 0.05$.

**Figure 3:** ***In vitro*** **effect of Pyr1 on invasion.**

**A**. Wound-healing assay. A white lane delineates the edges of the wound.

**B**. Quantification of speed, total displacement and persistence of cells at the wound edge, using the MTrackJ plugin from ImageJ software. Bars= SEM, n = 30 cells tracked per field, 3 fields per group. *** $p < 0.001$

**C**. Matrigel invasion assay. Histograms represent quantification (mean ± SEM) of invasion of TS/A-pGL3, MDA-MB-231 and MDA-MB-231-ZNF217rvLuc2 cells treated with 25µM Pyr1 or 0.25% DMSO, as described in the material and methods section, ** $p < 0.01$, *** $p < 0.001$.

**D**. Fluorescent images of MEF SrcY527F cells stably expressing LifeActRFP after 50 min of treatment with 0.25% DMSO or 25µM Pyr1. Bar, 10µm.

**E**. FRAP analysis of actin dynamics on MEF SrcY527F cells transfected with GFP-Actin and treated or not with 25µM Pyr1 as indicated. The characteristic time of recovery was quantified using the ZEN software from Zeiss. Bar = SEM, ***$p < 0.001$.

**Figure 4: Effect of Pyr1 on filopodium-like protrusions**

**A**. Bright field images of spheroids derived from MDA-MB-231 and MDA-MB-231-ZNF217rvLuc2 cells, incubated with 0.25% DMSO or 25µM Pyr1 for 2 hours. Bar, 20µm.

**B**. Average percentage of spheroids with FLPs in the absence (DMSO) or in the presence of 25 µM Pyr1, as indicated. Bars = SEM, * $p < 0.05$, ** $p < 0.01$.

**C**. Average length of FLPs. The length of FLPs was measured on 25 spheroids per treatment, in 3 independent experiments. Bars= SEM, * $p < 0.05$, ** $p < 0.01$, *** $p < 0.001$.

**Figure 5**: ***In vivo*** **analysis of Pyr1 effects on tissues and tumor cells characteristics.**

**A**. Representative intravital images of MDA-MB-231 Dendra2 tumors from mice treated with vehicle or 10 mg/Kg Pyr1 for at least 8 days. Three tile scans obtained from 3 different mice are shown. Upright inserts are 4X magnifications of regions of interest. Bar, 100µm.

**B**. Quantification of MDA-MB-231 cells in tumors. Dendra2 fluorescent signals were quantified as described in the material and methods section. Upper panel: examples of images analyzed; red lines, drawn by the software, separate the green fluorescent areas from the non-fluorescent areas. Bar, 100µm. Lower pannel: average ratios of Dendra2 fluorescent areas over non-fluorescent areas (mean ± SEM of at least 3 tumors analysis, 5 fields per tumor), * $p < 0.05$.

**C**. Representative images of Ki67 staining after 8 days of treatment. Bar, 50µm. Histograms represent quantification of Ki67 positive cells (mean ± SEM of 3 tumors analysis), * $p < 0.05$.

**D**. Representative images of TUNEL assay tumor staining after 8 days of treatment. Bar, 50µm. Histograms represent quantification of TUNEL positive cells (mean ± SEM of 3 tumors analysis), * $p < 0.05$.

**Figure 6: *In vivo* analysis of Pyr1 treatment on MDA-MB-231 Dendra2 human breast tumors using intravital microscopy.**

**A**. Effect of Pyr1 on the speed of the entire MDA-MB-231 Dendra2 cell population. 50 cells were tracked per tile scan, 4 tile scans per mouse. The analysis was performed on, at least, 3 mice per group. Histograms represent the mean speed ± SEM. * $p < 0.05$, *** $p < 0.001$.

**B**. Pyr1 effect on cell morphology. The number of rounded cells was measured on 5 tile scans per mouse and expressed as a percentage of the total fluorescent cell number. The analysis was performed on3 mice per group. Histograms represent the mean percentage ± SEM. *** $p < 0.001$.

**C**. Pyr1 effect on the speed of rounded and elongated cells. The speed was measured as in A. Histograms represent the mean speed ± SEM. * $p < 0.05$, *** $p < 0.001$.

**D**. Pyr1 effect on the total displacement of rounded and elongated cells. The displacement was measured by tracking the cells, as described in A. Histograms represent the mean distance covered ± SEM. * $p < 0.05$, *** $p < 0.001$.

**E**. Pyr1 effect on the persistence of migration of rounded and elongated cells, measured by tracking the cells as described in A. Histograms represent the mean persistence ± SEM.*** $p < 0.01$.

**F**. Representative images of rounded cell migration in MDA-MB-231 tumors treated with Pyr1 (10mg/Kg). Two cells, respectively circled in yellow and in red, were tracked.

Rightmost panel shows a still image at t = 0 min with an overlay of the cumulative centroid tracks of the rounded cells. Bar, 20µm.

**Figure 7: Analysis of Pyr1 effect on metastasis establishment**

**A**. Representative images of Dendra2 fluorescence in lung sections, of mice bearing MDA-MB-231 Dendra2 mammary tumors, treated (Pyr1) or not (vehicle). Bar, 100µm.

**B**. Quantification of metastasis number. Histograms represent the average number ± SEM of metastasis nodules in the lung of mice treated with vehicle or 10 mg/Kg Pyr1. n = 6 fields per lung, 3 mice per group.

**D**. Effect of Pyr1 on MDA-MB-231-ZNF217rvLuc2 metastatic colonization. MDA-MB-231-ZNF217rvLuc2 cells stably expressing luciferase were injected in the blood stream. Metastases colonization was followed by bioluminescence. Histograms represent the average number ± SEM of metastatic sites, quantified on the bioluminescence images.

**E**. Quantification of total metastatic load using bioluminescence.

At day 35, the vehicle treated mice were sacrificed and the treatment with Pyr1 was stopped for the other group. Bars = SEM, n = 10 mice for each group. ** $p < 0.01$.

**F**. Representative bioluminescence images of one mouse per condition, treated (Pyr1) or not (vehicle) are presented.

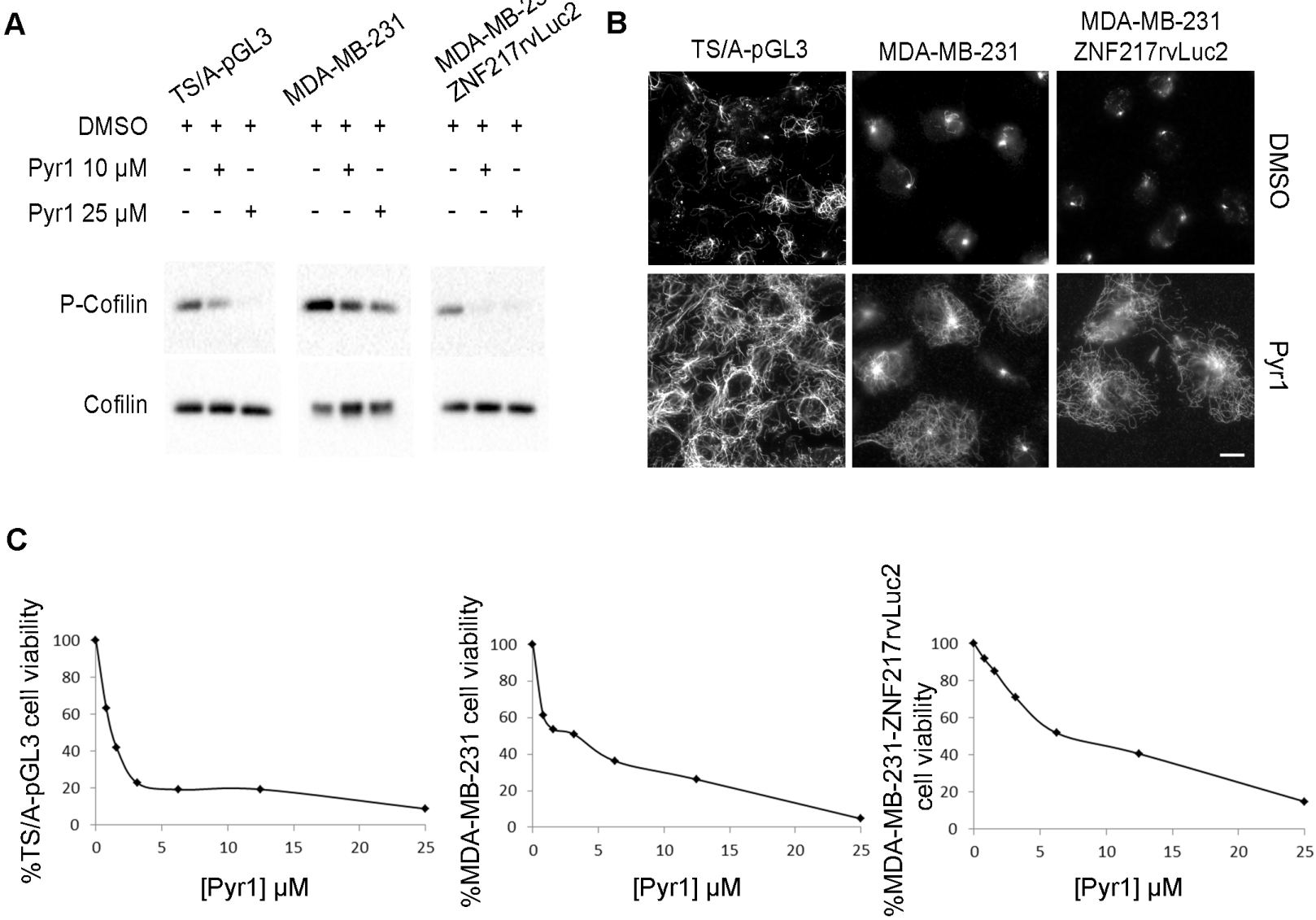
A
TS/A-pGL3
MDA-MB-231
MDA-MB-231 ZNF217rvLuc2
DMSO + + + + + + + + +
Pyr1 10 µM - + - - + - - + -
Pyr1 25 µM - - + - - + - - +
P-Cofilin
Cofilin
B
TS/A-pGL3
MDA-MB-231
MDA-MB-231 ZNF217rvLuc2
DMSO
Pyr1
C
%TS/A-pGL3 cell viability
%MDA-MB-231 cell viability
%MDA-MB-231-ZNF217rvLuc2 cell viability
[Pyr1] µM
[Pyr1] µM
[Pyr1] µM

**Figure 1**

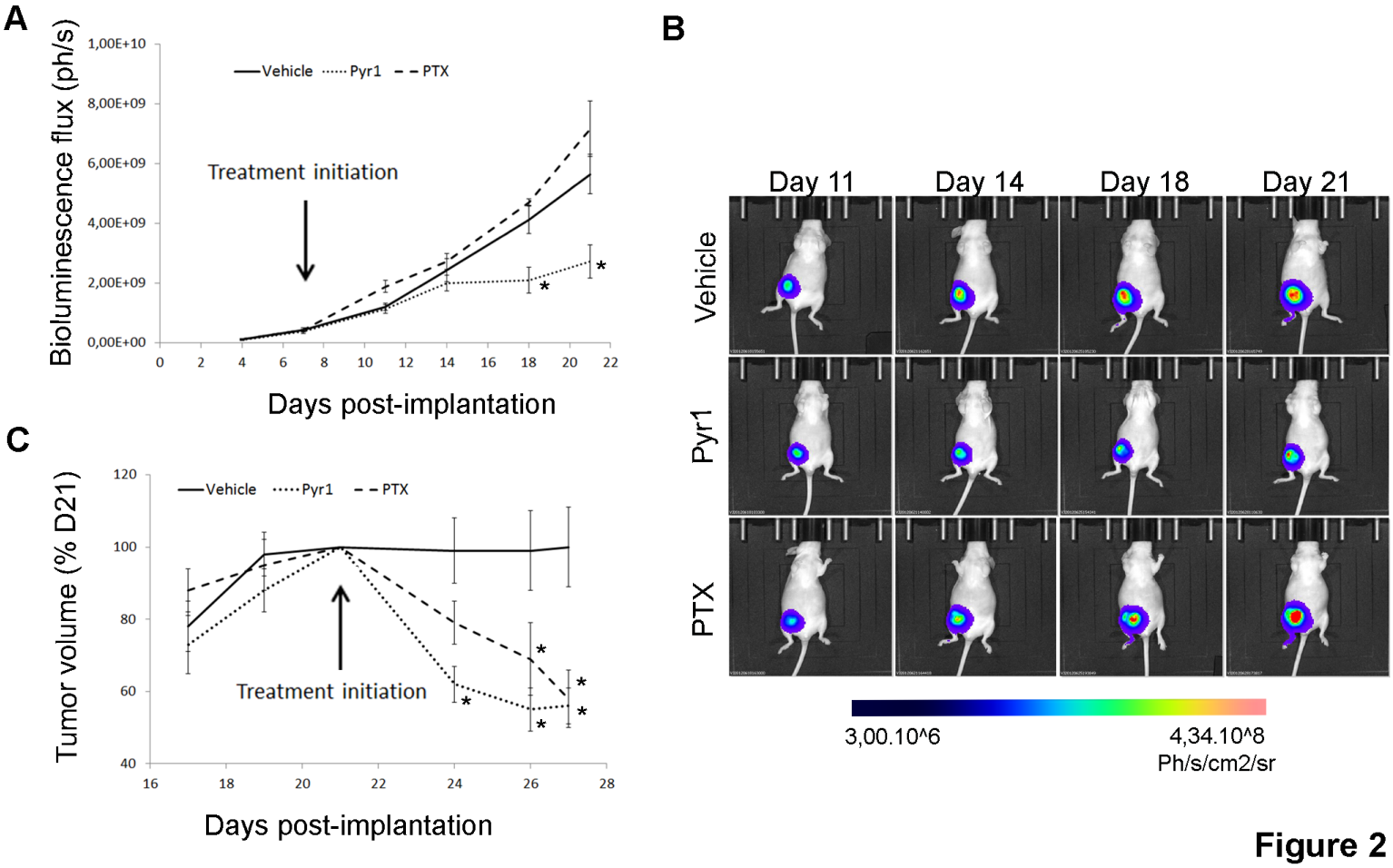
A
Bioluminescence flux (ph/s)
1,00E+10
8,00E+09
6,00E+09
4,00E+09
2,00E+09
0,00E+00
Vehicle
Pyr1
PTX
Treatment initiation
0
2
4
6
8
10
12
14
16
18
20
22
Days post-implantation
B
Day 11
Day 14
Day 18
Day 21
Vehicle
Pyr1
PTX
3,00.10^6
4,34.10^8
Ph/s/cm2/sr
C
Tumor volume (% D21)
120
100
80
60
40
Vehicle
Pyr1
PTX
Treatment initiation
16
18
20
22
24
26
28
Days post-implantation

**Figure 2**

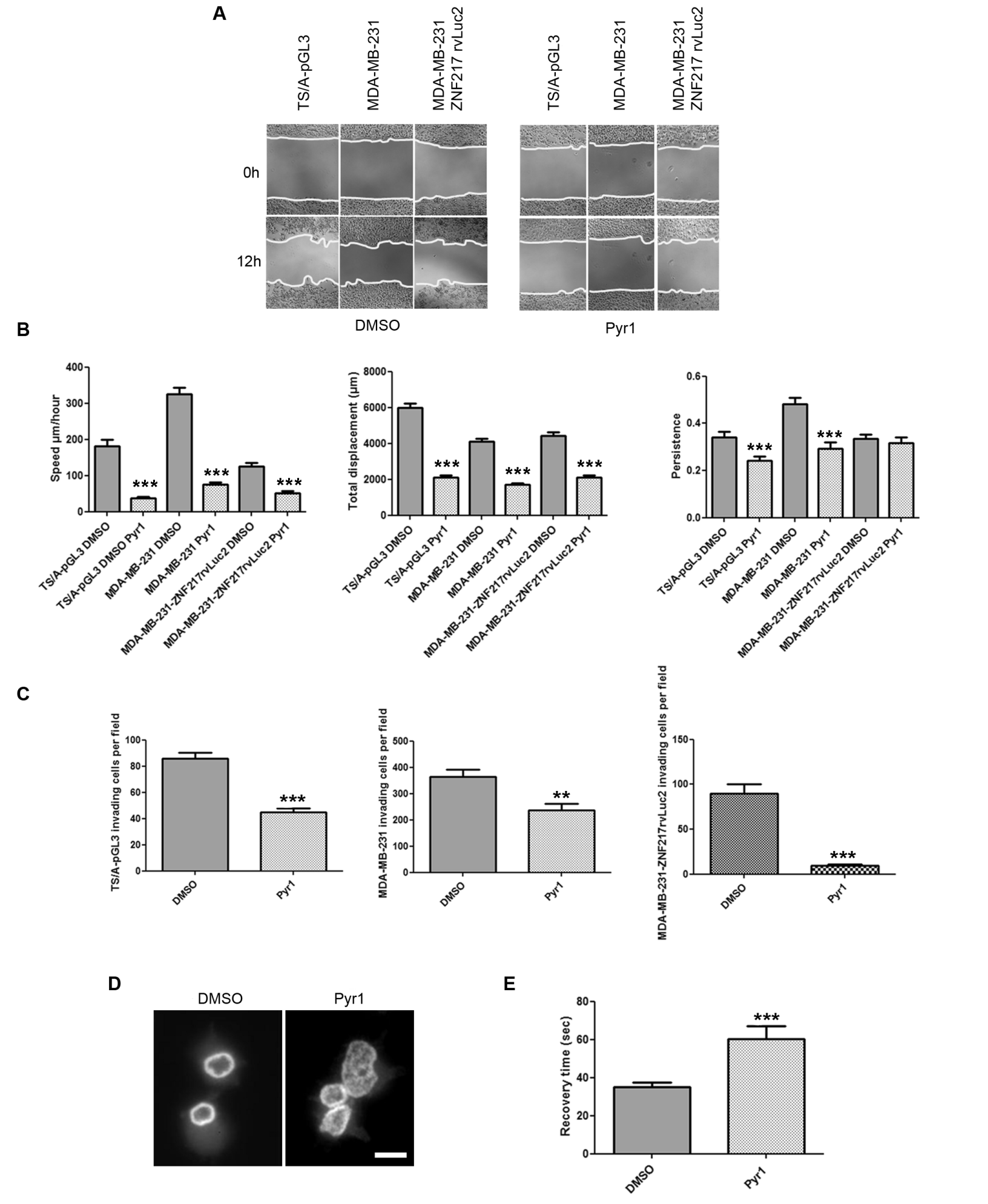
A
TS/A-pGL3
MDA-MB-231
MDA-MB-231 ZNF217 rvLuc2
TS/A-pGL3
MDA-MB-231
MDA-MB-231 ZNF217 rvLuc2
0h
12h
DMSO
Pyr1
B
Speed µm/hour
Total displacement (µm)
Persistence
TS/A-pGL3 DMSO
TS/A-pGL3 DMSO Pyr1
MDA-MB-231 DMSO
MDA-MB-231 Pyr1
MDA-MB-231-ZNF217rvLuc2 DMSO
MDA-MB-231-ZNF217rvLuc2 Pyr1
C
TS/A-pGL3 invading cells per field
MDA-MB-231 invading cells per field
MDA-MB-231-ZNF217rvLuc2 invading cells per field
DMSO
Pyr1
D
DMSO
Pyr1
E
Recovery time (sec)
DMSO
Pyr1

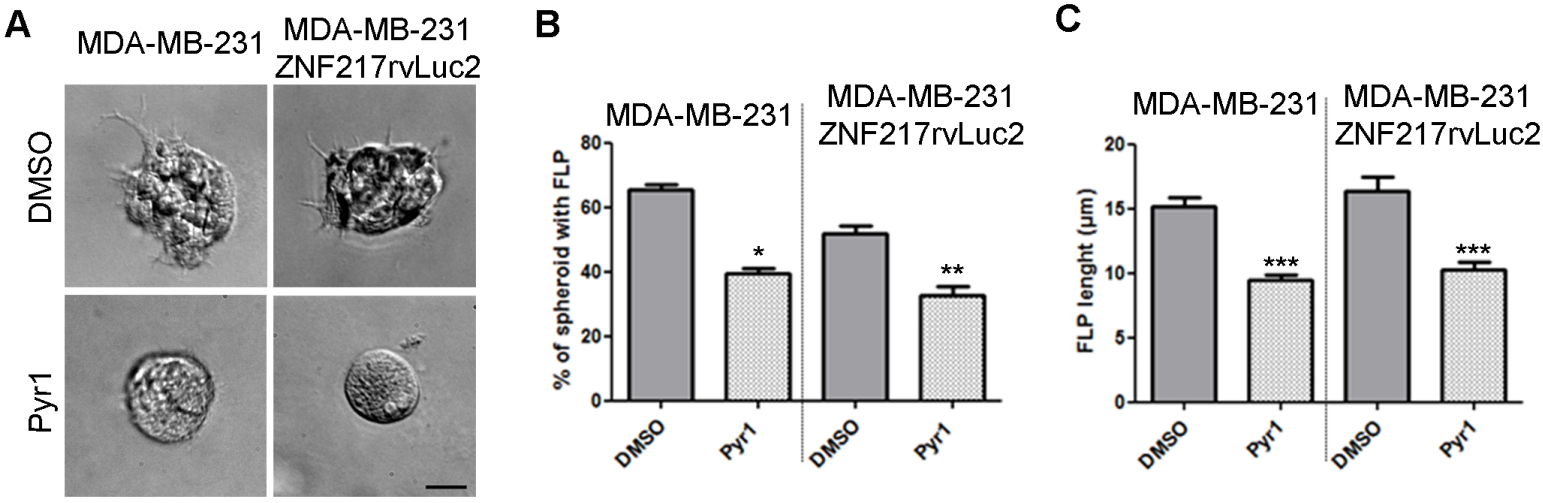
A
MDA-MB-231
MDA-MB-231
ZNF217rvLuc2
DMSO
Pyr1
B
MDA-MB-231
MDA-MB-231
ZNF217rvLuc2
% of spheroid with FLP
80
60
40
20
0
*
**
DMSO
Pyr1
DMSO
Pyr1
C
MDA-MB-231
MDA-MB-231
ZNF217rvLuc2
FLP lenght (µm)
20
15
10
5
0
***
***
DMSO
Pyr1
DMSO
Pyr1

**Figure 4**

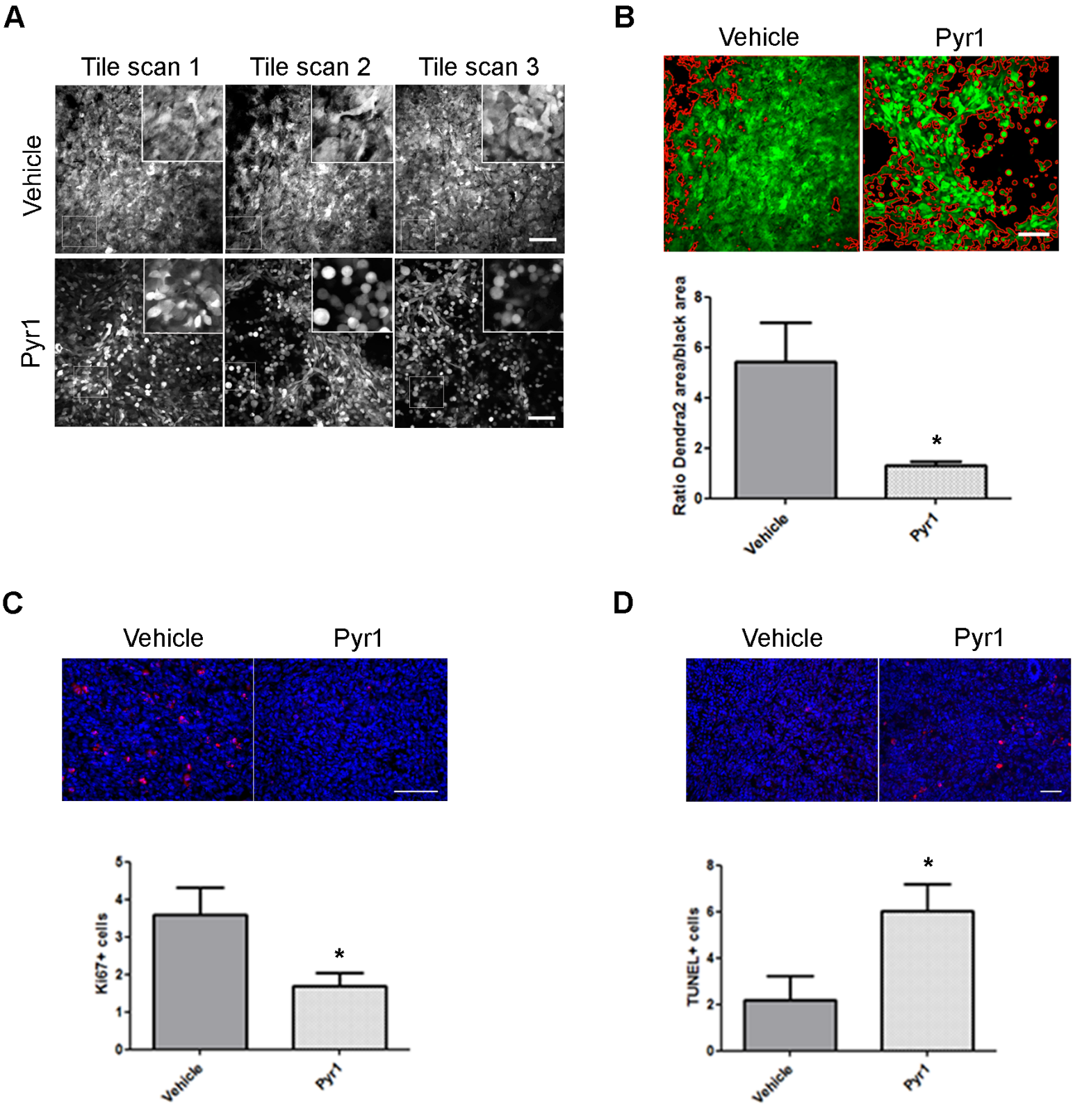
A
Tile scan 1
Tile scan 2
Tile scan 3
Vehicle
Pyr1
B
Vehicle
Pyr1
Ratio Dendra2 area/black area
0
2
4
6
8
*
Vehicle
Pyr1
C
Vehicle
Pyr1
Ki67+ cells
0
1
2
3
4
5
*
Vehicle
Pyr1
D
Vehicle
Pyr1
TUNEL+ cells
0
2
4
6
8
*
Vehicle
Pyr1

**Figure 5**

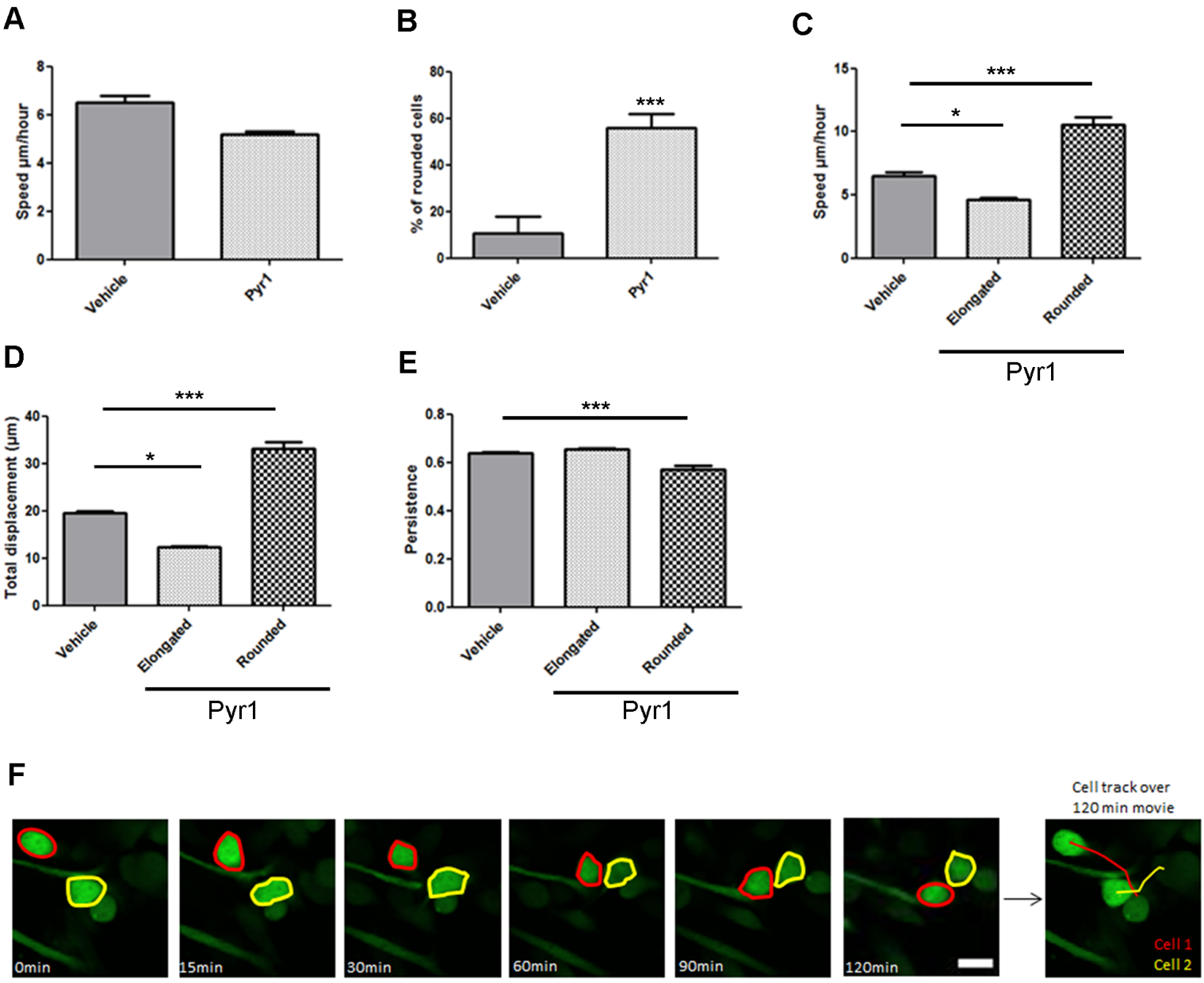
A
Speed µm/hour
0
2
4
6
8
Vehicle
Pyr1
B
% of rounded cells
0
20
40
60
80
***
Vehicle
Pyr1
C
Speed µm/hour
0
5
10
15
***
*
Vehicle
Elongated
Rounded
Pyr1
D
Total displacement (µm)
0
10
20
30
40
***
*
Vehicle
Elongated
Rounded
Pyr1
E
Persistence
0.0
0.2
0.4
0.6
0.8
***
Vehicle
Elongated
Rounded
Pyr1
F
0min
15min
30min
60min
90min
120min
Cell track over
120 min movie
Cell 1
Cell 2

**Figure 6**

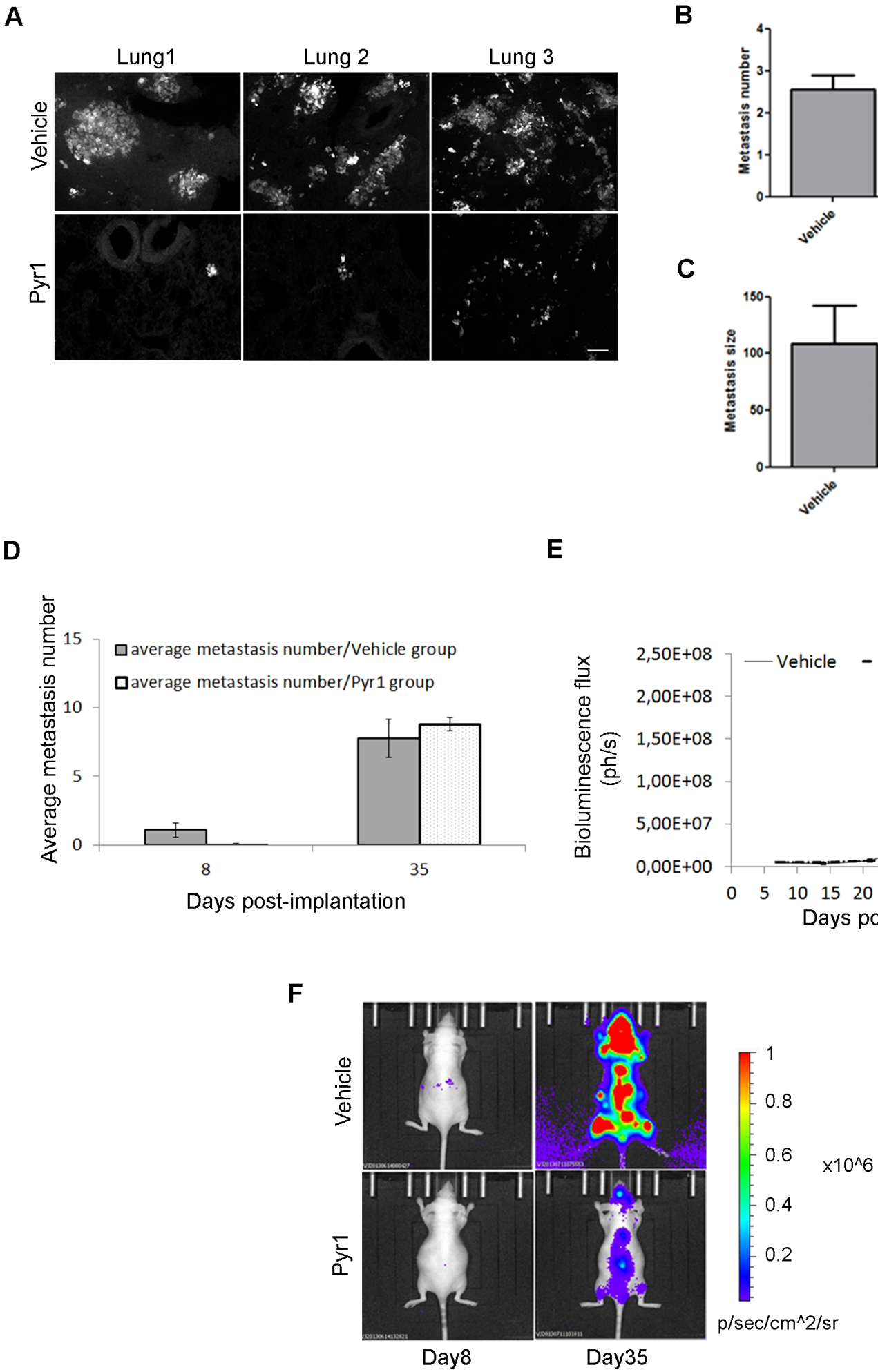
A
Lung1
Lung 2
Lung 3
Vehicle
Pyr1
B
Metastasis number
Vehicle
Pyr1
C
Metastasis size
**
Vehicle
Pyr1
D
Average metastasis number
average metastasis number/Vehicle group
average metastasis number/Pyr1 group
Days post-implantation
E
Treatment stop
Vehicle
Pyr1
Bioluminescence flux (ph/s)
**
Days post-implantation
F
Vehicle
Pyr1
Day8
Day35
x10^6
p/sec/cm^2/sr

**Figure 7**